Research Square

Preprints are preliminary reports that have not undergone peer review.
They should not be considered conclusive, used to inform clinical practice,
or referenced by the media as validated information.

Surface coating biomaterials shape morphology, transcriptomic identity, and excitability of human iPSC-derived nociceptors

Buket Ucar
Medical University Innsbruck
David Zimmermann
Medical University Innsbruck
Ferenc Török
Medical University Innsbruck
Georg Kern
Medical University Innsbruck
Kai K. Kummer
Medical University Innsbruck
Karolina Pircs
Semmelweis University
Attila Szücs
Semmelweis University
Michaela Kress
michaela.kress@i-med.ac.at

Medical University Innsbruck

Article

Keywords: iPSC-derived nociceptors (iNocs), MEA recording, neuron excitability, transcriptomic profiling, extracellular matrix

Posted Date: November 9th, 2026

DOI: https://doi.org/10.21203/rs.3.rs-11207616/v1

License: This work is licensed under a Creative Commons Attribution 4.0 International License.
Read Full License

Additional Declarations: No competing interests reported.

Surface coating biomaterials shape morphology, transcriptomic identity, and excitability of human iPSC-derived nociceptors

Buket Ucar[#1], David Zimmermann[#1], Ferenc Török[#1], Georg Kern[1], Kai Kummer[1], Karolina Pircs[2, 3, 4], Attila Szücs[2, 3, 5] & Michaela Kress[1*]

[#]equal contribution

[1]Institute of Physiology, Medical University Innsbruck, Austria

[2]Institute of Clinical Pathophysiology, Semmelweis University, 1094 Budapest, Hungary.

[3]Hungarian Centre of Excellence for Molecular Medicine - Semmelweis University (HCEMM-SU), Neurobiology and Neurodegenerative Diseases Research Group, 1094 Budapest, Hungary.

[4]HUN-REN-SZTAKI-SU Rejuvenation Research Group, HUN-REN Office for Supported Research Groups (TKI), 1052 Budapest, Hungary.

[5] Department of Physiology and Neurobiology, Institute of Biology, Eötvös Loránd University, 1117 Budapest, Hungary.

[*]corresponding author
Univ.-Prof. Dr. Michaela Kress
Institute of Physiology
Medical University Innsbruck
Schöpfstr. 41
6020 Innsbruck
Austria
E-Mail: michaela.kress@i-med.ac.at
Phone: +43 512 9003 70800
Mobile: +43 699 18351155
Fax: +43 512 9003 73800

Key words: iPSC-derived nociceptors (iNocs), MEA recording, neuron excitability, transcriptomic profiling, extracellular matrix

Abstract

Human induced pluripotent stem cell (iPSC)-derived nociceptors (iNocs) are valuable tools for modelling sensory neurobiology and pain, while achieving maturation and reproducibility remains challenging. Currently available differentiation protocols focus on soluble factors, but the role of the extracellular matrix is insufficiently understood. In this study we investigated how widely used plastic surface coatings including laminin, poly-L-lysine/laminin and Matrigel™ influenced the morphology, transcriptional identity, and functional activity of human iNocs combining indirect immune fluorescence microscopy, RNA sequencing, multi-electrode array recordings and single-cell patch-clamp techniques. Significant differences were obtained in iNocs morphology, the size of cellular clusters, and transcriptomic signatures. Matrigel coating promoted biological gene ontologies related to "extracellular matrix remodelling" and "mesenchymal pathways" whereas laminin coating enhanced neuronal and synaptic processes and enriched proliferative gene sets. Spontaneous discharge activity was increased in iNocs cultured on poly-L-lysine/laminin exhibiting the highest firing rates. Single cell patch clamp recordings revealed minor effects of coating materials on passive membrane properties and basic electrophysiological parameters of individual iNocs. These findings introduce coating specific extracellular matrix compositions as a critical regulator of iNoc phenotypes. Optimizing surface coating substrates offers a powerful strategy to improve the physiological relevance and maturation of translational human pain models.

1. Introduction

Somatosensory primary afferent neurons form the first processing level in the pain pathway, with nociceptors whose cell bodies are located in dorsal root (DRG) and trigeminal ganglia (TG), representing a heterogeneous neuronal population, specialized to detect noxious thermal, mechanical, and chemical stimuli and transmit signals to the spinal dorsal horn and higher brain centres. Nociceptor diversity is reflected by distinct molecular markers, neurotrophin receptor expression, ion channel profiles, and transcriptional signatures which characterise multiple mechanoreceptor, proprioceptor, and peptidergic or non-peptidergic nociceptor subtypes[1–4]. However, human nociceptor transcriptomes differ substantially from those of rodents, with broader neurofilament heavy polypeptide (NEFH) expression, enrichment of peptidergic phenotypes, and conserved *TrkA* and *Nav1.8* expression defining major human nociceptor populations[5–9]. Research on human nociception has historically been limited by restricted accessibility and species-specific differences between animal models and humans. Human induced pluripotent stem cell (iPSC)-derived nociceptors (iNocs) provide a powerful platform to overcome these limitations[10,11]. Differentiation protocols typically rely on dual-SMAD inhibition combined with small-molecule signalling modulation (CHIR99021, SU5402, DAPT), followed by neurotrophic factor-mediated maturation[11,12]. These approaches generate neurons expressing sensory lineage markers such as *BRN3A* and *ISL1* and nociceptor-associated ion channels including *SCN9A*, *SCN10A*, and *TRPV1*[10,12–14]. Although the protocol developed by Chambers et al. is considered the gold standard, variations in differentiation timing, growth factor composition, or additional signalling pathways can generate diverse sensory neuron subtypes including mechanoreceptors and proprioceptors. [12]. Despite recent advances, iNoc models remain limited by incomplete maturation, heterogeneous subtype composition, and variability between differentiation protocols. Importantly, most differentiation strategies focus on soluble signalling cues, whereas the physical and biochemical microenvironment is often underappreciated as a determinant of neuronal identity and function.

In vivo, neurons interact with a complex extracellular matrix (ECM) environment and perineuronal nets that regulate neuronal survival, maturation, synapse formation, and electrophysiological properties [15]. Sensory neurons express subtype-specific integrin profiles, and different neuronal populations respond differently to ECM substrates [16]. ECM composition is increasingly recognized as a regulator of synapse development and neuronal maturation for iPSC-derived cortical neurons[17–20]. Integrin-mediated interactions with ECM ligands such as

laminin, collagen, and fibronectin may directly influence neuronal maturation programs[18]. However, little is known about ECM–interactions in human sensory neuron differentiation and phenotypes[21,22]. If critical extracellular interactors are absent, iNocs may fail to initiate or maintain essential maturation programs, resulting in transcriptomic and functional deficits compared to native nociceptors[6,11,13]. Consistent with this concept, iNocs frequently show low levels of spontaneous discharge activity, whereas native sensory neurons typically remain electrically silent in the absence of stimulation[10].

In vitro, various surface coating materials are widely used to support neuronal adhesion and differentiation. Commonly used substrates include ECM proteins such as laminin, collagen, and fibronectin, complex mixtures such as Matrigel, and synthetic polycations such as poly-L-lysine (PLL) or poly-L-ornithine (PLO). These coatings influence surface charge, topography, and cell–substrate interactions and thereby modulate cell attachment, morphological properties, neuronal survival and neurite outgrowth[23,24]. Although these materials are widely used in neuronal culture systems, their specific effects on nociceptor differentiation and maturation remain poorly characterized. Various studies differentiate iNocs using Matrigel[12,25], poly-L-ornithine/laminin[26], or alternative matrix coatings[27,28], but systematic comparisons remain limited.

We hypothesize that the physical and chemical microenvironment plays a critical role in regulating nociceptor phenotype, ion channel expression, and excitability. Specifically, ECM composition and surface coating materials may directly influence transcriptional programs governing neuronal maturation, signal propagation, and responsiveness to physiological stimuli. Optimizing substrate composition may therefore represent a key strategy to improve the functional maturation and physiological relevance of iPSC-derived nociceptors. In this study, we investigated the effects of different culture surface coatings on the morphology, differentiation, and functional maturation of human iPSC-derived nociceptors. We specifically compared three commonly used coating materials in neuronal cell cultures, which are Matrigel, laminin, and PLL/laminin (LA), and compared their impact on transcriptomic profiles, ion channel expression, and neuronal excitability. By systematically evaluating how extracellular microenvironmental factors influence nociceptor development, this work aims to improve the physiological relevance of iPSC-derived nociceptor models and improve the functional similarity of human iPSC derived *in vitro* systems and native human sensory neurons.

Experiments

All methods were carried out in accordance with relevant guidelines and regulations. All iPSC clones were obtained by and used under the ethical regulations of the STEMBANCC consortium. All animal procedures followed the guidelines of the International Association for the Study of Pain, the EU Directive 2010/63/EU for animal experiments and the National Institutes of Health Guide for the care and use of laboratory animals and were approved by the Austrian Bundesministerium für Frauen, Wissenschaft und Forschung BMFWF (BMWF-66.011/0102-WF/V/3b/2015) and by the local Institutional Animal Care and Use Committee at IPHYS (Project No 78–2024-P).

iNoc differentiation

Adult 840 clone iPSCs derived from a healthy patient with no history of diseases were used for standardized experiments and iNocs differentiation performed as published[10,12]. Briefly, approximately 80 x 10^3 cells per 6-well were seeded as single-cells, two passages after thawing. Cells were maintained overnight in mTeSR+ medium containing Y-27632 (Sigma-Aldrich) until 60-70% confluency. Subsequently dual-SMAD inhibition was initiated in knockout serum replacement media (KSR) supplemented with 100 nM of LDN-1931189 and 10 µM SB431542 for 5 days. Additionally, three µM CHIR99021, 10 µM DAPT and 10 µM SU5402 were added from day 2- day 12. From day 4 on N2/B27 (Neurobasal medium/GLUTAMAX/B27/N2) was added to the KSR media and incremented every 2 days by 25%. On day 12, cells were passaged onto glass coverslips with different coatings for immunofluorescence experiments and maintained in N2/B27 medium supplemented with NGF, BDNF and GDNF. Cytosine-β-D-arabinofuranoside (Sigma Aldrich) was administered on day 14 for ~24h to reduce the amount of non-differentiated proliferating cells. Cells were maintained until day 26, medium was changed every second-third day. iNocs were seeded on the following coatings on day 12: Matrigel™, fibronectin (10 µg/ml), thrombospondin-1 (10 µg/ml), PLL-laminin (Laminin 1 µg/cm2; PLL 1 µg/cm2), collagen type 1 (0.1 mg/ml), biosilk 521 (Biolamina, 0.3 mg/ml) and maintained in N2/B27 medium supplemented with NGF (25 ng/ml), BDNF (10 ng/ml) and GDNF (10 ng/ml) until day 26 or day 36. Morphological changes were recorded.

Immunohistochemistry

Cells were fixed with 4% PFA for 15 min at room temperature (RT) at day 26 or day 36. Fixed iNocs were washed 3x with PBS, permeabilized and blocked for 1 h in 0.2% Triton-PBS (T-PBS) with 0.2% BSA and 5% normal goat serum at RT. Primary antibodies were applied at 4°C overnight, in a humidified chamber, Tuj1 (1:1,000, R&D Systems, #MAB1195), SOX10(1:1000, Cell Signaling Technologies, #89356). After subsequent washing 3x with

PBS, the slices were incubated with secondary antibodies for 1 h and counterstained with DAPI (Thermo Fischer, #D1306). Secondary antibody for SOX-10 (Z01, Thermo Fischer, A-11029) was also applied in the concentration of 1:500. Samples were washed and mounted in Mowiol. Since cells that were not fully differentiated exhibited larger DAPI+ nuclei and were not stained by the neuronal marker Tuj1. All fluorescent images were acquired with Olympus IX83 microscope. DAPI staining quantification was automatized with ImageJ by using a global filter. Tuj1+ cells were manually counted with the help of cell counter notice plugin in ImageJ. The normalized Tuj1/DAPI fluorescence intensity ratio was calculated as a gross measure of differentiation. Average fluorescence intensities were quantified using ImageJ software with a global threshold. The same size of region of interest (ROI) was used in each image that is placed in the middle of the coverslip (at least 1 mm away from the sides) on a region completely covered with cells. Total cell number was determined by automatized counting of DAPI staining to evaluate cell attachment to the surface.

Sample preparation for RNA sequencing

Differentiated nociceptors (day 12) were passaged onto accordingly coated 6-well cell culture plates (Greiner 657160) at a seeding density of approx. 50,000 cells/cm^2. Starting 24 hours later, cells were treated with 4 µM Cytosine β-D-arabinofuranoside (Ara-C; Sigma C1768) for 48 hours to suppress growth of contaminating cells. Cultures received half-feeds with maturation medium three times a week. At day 36, cells were harvested with Accutase™ (Gibco A1110501), washed two times with ice-cold PBS, and snap frozen as pellets by placing the tubes in liquid nitrogen. Samples were stored at -80°C until shipping on dry-ice for analysis.

RNA extraction and sequencing

RNA extraction, quality control, library preparation, and sequencing were performed by Lexogen GmbH (Vienna, Austria). Total RNA was extracted from cell pellets using the SPLIT RNA Extraction Kit (Lexogen). RNA concentration and integrity were assessed using a Fragment Analyzer (Agilent Technologies, USA), with RNA Quality Numbers (RQN) ranging from 9.3 to 10.0. Sequencing libraries were prepared using the QuantSeq V2 library preparation protocol (Lexogen), with 350 ng total RNA per sample. Libraries were multiplexed and sequenced on an Illumina NextSeq 2000 platform using single-end 100 bp sequencing. Sequencing yielded an average of 9.66 million reads per sample (range: 8.40-10.21 million reads). Raw sequencing data were deposited in the European Nucleotide Archive (ENA) under accession number PRJEB128515.

RNA-seq data sets and bioinformatics analysis

Raw sequencing reads quality and phred quality scores were assessed manually using *fastqc* (v. 0.11.9). The overall raw read length was 100 bp. The raw sequencing reads were deduplicated to reduce the impact of amplification bias using *umi-tools* (vers. 1.1.4). Low quality bases and adaptor sequences were trimmed using *bbduk* (BBMap v. 38.18) with trimming parameters set to kmer size = 13, use of shorter kmers enabled and the minimum kmers threshold was set to 5. Quality trimming was enabled to remove reads with a read length smaller than 20 nucleotides and base pairs with a quality score < 10. Deduplicated sequencing reads were aligned against the human reference genome (Gr38) using STAR-aligner (v. 2.7.0). Remaining PCR duplicates were removed in a second deduplication step performed using umi-tools. The raw transcript counts per gene were processed into a count matrix using feature counts of the Rsubread package (v 2.12.3) in R (v. 4.2.2). Low expressed genes with a threshold <10 counts were removed from the count matrix and differentially regulated genes were identified using DESeq2 (v. 1.38.3)[29]. To correct for multiple testing, false detection rate (FDR) correction was performed using the Benjamini-´Hochberg algorithm resulting in adjusted p-values (p-adj). Gene-Ontology enrichment analysis (GO) was performed using ClusterProfiler (v 4.6.2) for genes with p-adj<0.0 1. Before GO, genes were ranked according to the product of log2foldchange*(-log10(p-adj)).

Multi-Electrode Array (MEA) Recordings

iNoc cultures were generated from iPSCs as described above followed by re-plating on CytoView 24 well MEA plates (Axion Biosystems) coated with Matrigel™, laminin and PLL/laminin (8 wells of each coating) on day 12 and kept as described until day 45. Recordings of electrical spontaneous activity were executed on the Maestro Edge MEA system (Axion Biosystems) every day at the same time for 1 h at 37°C and 5 % CO^2. Cells were allowed to recover for 5 min from the transfer of the 24-welll plate from the incubator to the MEA system prior the recording was started. Every 2-3 days, half of the medium was changed carefully to reduce medium change introduced batch effects on the cultures and to retain comparability of the recordings between different time points. Data was evaluated at per-electrode and per-well level by combining the data from 16 electrodes in each well. In addition, data for active electrodes were evaluated separately, where an active electrode was defined as more than 1 spike per 10 min during the whole recording time to exclude electrodes without contact with cells or cells with no spontaneous activity. Action potentials were detected using the threshold crossing method implemented in the Axis software, and the threshold level was set to 6-times

to that of the standard deviation of the recorded voltage signal. The resulting spike trains were analyzed by the Axis program as well as NeuroExpress developed by ASz.[30]

Patch-clamp recordings

To assess the effect of coating materials on electrophysiological properties cells were seeded on 35 mm dishes (Thermo Fischer Scientific, cat.nr. 153066) coated either with Matrigel or PLL/Laminin and kept in sterile incubator at 37°C and 5% CO_2. Cell adhesion on laminin alone was not sufficient and therefore laminin alone was not further pursued. Patch-clamp recordings were performed on day 40-41 with patch pipettes from borosilicate glass (GB120-8P, Scientific Products, Hofheim, Germany) pulled with an automated puller (Sutter Instruments, Novaton, CA, USA) to a final resistance of 4.0–5.0 MΩ. Recording solutions contained (in mM): *bath solution*: 2 $CaCl_2$, 10 HEPES, 145 NaCl, 1 $MgCl_2$, 5 KCl, 10 glucose adjusted to pH = 7.3 with NaOH; *pipette solution*: 10 HEPES, 5 EGTA, 98 K-Gluconate, 45 KCl, 2 Mg-ATP, 0.2 Na-GTP, 0.5 $CaCl_2$, 2 $MgCl_2$, adjusted to pH = 7.3 with KOH. Recordings were performed on room temperature (20–24°C) using EPC-10 USB (HEKA). Signals were low pass filtered at 1 kHz and sampled at 20 kHz. The resting membrane potential (RMP) was measured in whole-cell current clamp configuration. Recordings with leak currents >200 pA were excluded. Recordings were analysed using Fitmaster v2x90.3, Clampfit 11.4.3 (Axon Instruments, San José, CA, USA) and GraphPad Prism 8.0.1. Current densities were obtained by normalizing inward or outward currents to cell size (pA/pF). Leak subtraction was done online by P/4 protocol. Current–voltage (I–V) relationships were obtained for whole cell inward and outward currents evoked by 50-ms square pulse depolarizations from the holding potential of -60 mV to different test potentials in the increment of 5 mV to +40 mV and data were fitted to the following equation:

$$I=G_{max}*(V-V_{rev})/(1+\exp^{f_0}(-(V-V_{0.5,act})/k_{act})$$

where V_{rev} is the extrapolated reversal potential, V is the test potential, G_{max} is the maximum slope conductance, $V_{0.5,act}$ is the voltage of half-maximal activation, and k_{act} is the activation slope factor.

Statistical analysis

For statistical analyses, GraphPad Prism 10.0.1 (GraphPad Software, USA) was used as applicable. All results are presented as mean ± SEM, n indicates number of coverslips or number of images that are used in the analysis and indicated for each graph. Initial microscopy analyses were all compared to Matrigel (One-way ANOVA with Multiple comparisons).

Analyses were performed by comparing each coating to each other and the respective timelines (two-way ANOVA with Multiple comparisons). For group comparisons, the Mann-Whitney u-test was used with Bonferroni's post-hoc test. The level of statistical significance was predefined at $p < 0.05$.

Results

Morphological differences induced by different coating materials

Initially we compared the effect of individual and combined coating materials, namely Matrigel, poly-L-lysine/laminin (PLL/LA), Fibronectin, collagen, Biosilk™, laminin, thrombospondin, carbon/PLO, PLO/Matrigel, Carbon/gelatin and Carbon/gelatin/Matrigel on cellular morphology and expression of the neuronal marker Tuj1 (**Fig. 1**) in 2 or 3 replicates per condition. Most coatings provided good attachment to maintain iNocs from day 12 until day 26. Cells seeded on thrombospondin detached around day 18. In about half of the cultures (3 out of 6) on collagen coating attachment of the cells was also lost and cultures on carbon/gelatin coated coverslips developed detached areas, causing a significantly smaller percentage of Tuj1+ area per coverslip (**Fig. 1D**).

Normalized Tuj1/DAPI fluorescence intensity ratio was higher for cultures on collagen and Biosilk vs. Matrigel, however, similar between all other groups. Matrigel coating yielded significantly more DAPI+ particles compared to laminin and carbon/gelatin/Matrigel coating and similar cell attachment for the remaining coating materials. Furthermore, we evaluated the ratio of Tuj1+ to DAPI staining and observed that Biosilk™ and laminin resulted in a significantly higher percentage compared to Matrigel (66.8% [Matrigel] vs 79.69% [silk], and 79.46% [laminin], $p = 0.0093$ and 0.0137, One-way ANOVA).

In general, iNocs form clusters rather than spread out as individual cells[31]. We next assessed whether coating materials such as collagen and carbon/gelatin prompted the cells to cluster together in lower or larger numbers (**Fig. 2A**). We evaluated the ratio of single neurons over the total number of clusters, and the number of cells in each cluster by using Tuj1+ staining. A cluster was defined as 2 or more cell somata with direct contact. Overall, most iNocs were clustered and the number of Tuj1+ neurons that were not in any clusters was approximately 20% in all conditions (**Fig. 2B**). The number of Tuj1+ clusters was highest in cultures on PLL/laminin coating; and compared to Matrigel™ was significantly lower in iNocs cultures on fibronectin, collagen, laminin, carbon/gelatin and carbon/gelatin/Matrigel coatings. These differences may be due to either fewer clusters with larger cell numbers or more single cells compared to clusters. To discriminate these possibilities, we evaluated the mean number of cells in each cluster. While iNocs cultures on most evaluated coatings contained on average 4 cells in each cluster, cells cultured on collagen and carbon/gelatin developed significantly larger clusters compared to Matrigel (**Fig. 2B**). Specifically, collagen coating caused formation

of clusters with more than 20 cells often and clusters on carbon/gelatin coating exceeded 50 cells per cluster. Large clusters were surrounded by neurite bundles, while cultures with less clustering generate a more diffuse pattern of neurite growth.

Transcriptomic Differences induced by coating substrates

iNocs growing on LA, PLL_LA and Matrigel™ coating were bulk mRNA sequenced (n = 4 per condition) to assesses the impact of coating materials on the transcriptomic profile of iNocs. Principal component analysis (PCA) of rlog-transformed counts revealed clear transcriptional separation between the three coating conditions (**Fig. 3A**). The first principal component (PC1) explained 53.77% of the total variance, while PC2 explained 28.83%**,** together accounting for over 80% of total transcriptomic variance. These results indicated that substrate coating seemed to be a dominant driver of global transcriptional identity. Sample-to-sample distance analysis confirmed strong clustering by coating condition, demonstrating high intra-condition similarity and distinct inter-condition transcriptional profiles. Likelihood ratio testing identified 2,591 genes significantly regulated genes across coating conditions (adjusted p-value<0.05), highlighting the extensive transcriptional response to substrate composition. Pairwise comparison between Matrigel and LA identified 1,688 differentially expressed genes (DEGs), including 735 genes upregulated and 953 genes downregulated in Matrigel™ relative to LA (**Fig. 3B**). Pairwise comparison of Matrigel™ and PLL_LA identified 431 DEGs, including 238 genes upregulated and 193 genes downregulated in Matrigel™ relative to PLL/LA (**Fig. 3C**). Pairwise ccomparison between PLL/LA and LA identified 2,445 DEGs, including 1,029 genes upregulated and 1,416 genes downregulated in PLL/LA relative to LA (**Fig. 3D**).

GO enrichment analysis of DEGs were higher in cells growing on Matrigel™ revealed strong enrichment of extracellular matrix (ECM) and adhesion-related processes, including extracellular structure organization, extracellular matrix organization, collagen fibril organization, integrin-mediated signalling, and cell-substrate adhesion. Developmental programs related to mesenchymal development and mesenchymal cell differentiation were also significantly enriched (**Fig. 4A**). In contrast, genes with higher expression profile in LA samples were strongly enriched for neuronal and synaptic processes, including axon development, synapse organization, axonogenesis, neurotransmitter transport, and regulation of synaptic signalling (**Fig. 4B**). These data suggest that Matrigel™ seemed to promote ECM remodelling and adhesion-associated transcriptional programs while suppressing neuronal

lineage-associated transcriptional signatures compared to LA. Matrigel™ upregulated genes were enriched primarily for ECM organization, extracellular structure organization, and collagen fibril organization, consistent with ECM remodelling as a defining transcriptional feature of Matrigel™. Interestingly, enrichment was also observed for glial lineage-associated processes including gliogenesis, myelination, and axon ensheathment (**Fig. 4D**). DEGs with higher expression in PLL/LA relative to Matrigel™ were enriched for neuronal developmental processes, including axonogenesis, axon guidance, neuron projection development, and neuronal migration (**Fig. 4E**). These findings suggest that PLL/LA seemed to maintain stronger neuronal lineage-associated transcriptional programs compared to Matrigel™, while Matrigel™ promoted ECM-dominant transcriptional states.

GO enrichment analysis of genes upregulated in PLL/LA revealed strong enrichment of cell cycle and mitotic processes, including mitotic nuclear division, chromosome segregation, sister chromatid segregation, and regulation of cell cycle phase transition (**Fig. 4G**). DEGs with higher expression in LA were enriched for synaptic and neuronal signalling processes, including synapse organization, modulation of chemical synaptic transmission, neurotransmitter secretion, axon development, and vesicle-mediated transport in the synapse (**Fig. 4H**). These results suggest a shift from neuronal/synaptic functions toward proliferative and mitotic activity in the PLL_LA condition.

During GO analysis, we noticed several DE ion channels, prompting a systematic evaluation of their expression across conditions. In the Matrigel™_vs_PLL/LA comparison, six ion channel genes were differentially expressed, including SCN9A (voltage-gated sodium channel), GLRA3 (glycine receptor), and GRIN2A/GRIN2B (NMDA receptor subunits), suggesting potential alterations in action potential initiation and excitatory synaptic transmission (**Fig. 4C**). The Matrigel™_vs_LA comparison revealed 21 differentially expressed ion channels, including SCN1A, SCN2A, SCN3B (sodium channels), KCNB1, KCNQ2, KCNK5, KCNK10, KCNH5 (potassium channels), CACNA1E, CACNB1 (voltage-gated calcium channels), and GABRA3, GABRB3, GABRG2, GLRA3 (GABA and glycine receptors). These changes likely modulate neuronal excitability, spike threshold, and inhibitory/excitatory balance, potentially affecting firing frequency and network synchronization in Matrigel™ compared to LA (**Fig. 4F**). In the PLL/LA vs. LA comparison, 35 ion channel genes were differentially expressed, including multiple sodium, potassium, calcium, and ligand-gated channels (*SCN1A*, *SCN2A*, *SCN8A*, *KCNK2*, *KCNK3*, *KCNB1*,

CACNA1A, *CACNA1B*, *CACNB3*, *GRIA1*, *GRIK2*, *GRIN2A/B*, *GABRA2*, *GABRA3*, *GABRG2*, *GLRA3*). These alterations suggest widespread modulation of membrane excitability, synaptic strength, and action potential propagation, which could impact network-level activity in PLL/LA relative to LA (**Fig. 4I**). Overall, these data indicated condition-specific remodelling of ion channel expression, pointing to potential functional consequences for neuronal excitability, synaptic integration, and circuit dynamics across the experimental groups.

Functional Differences induced by LA, PL/LA and Matrigel™

To assess the functional impact of DE ion channel profiles, MEA recordings were performed between D24 and D45 of iNoc culture. Also under these conditions, iNocs seeded on Matrigel™ were equally dispersed in small clusters, while neurons cultured on LA and PLL/LA formed large clusters with radial neurite outgrowth in large bundles (**Fig. 5**). These recordings demonstrated the overall stability and variability of spontaneous firing activity of iNoc cultures grown on 3 types of surfaces. While the intensity of firing activity significantly varied across wells and electrodes, consistent features were also identified. Importantly, iNoc cells recorded on separate electrodes within a well exhibit no synchronization in their firing output. This was recapitulated by the near zero values of Pearson's correlation calculated for pairs of active electrodes. Bursts or transient changes in firing were rarely observed. Instead, neurons maintained a spontaneous activity was fairly stable during the time of recording. For most recorded electrodes, iNocs exhibited a spontaneous firing pattern that was characterized by a Poissonian interspike interval distribution. Occasionally, we observed slow oscillatory activity manifested as 'waves' in the spike density functions calculated for the individual electrode channels (Fig 5A, 50-100 s periodicity). Yet, the spike trains recorded on different channels remained completely uncorrelated supporting the lack of synaptic connections or other means of network synchronization in the iNoc populations. With these attributes iNocs appeared to be similar to isolated native sensory neurons.

Mean spontaneous firing frequency (MFF) was assessed per electrode and normalized per well without additional stimulation. Low levels of spontaneous discharge activity developed after 24 days in culture for all three coating substrates and remained below 0.5 action potentials/s for all conditions. But significantly increased between D24 and D45 along all coating conditions MFF increase was most prominent in cultures on PLL/LA (0.05 spikes/s d24 vs 0.3 spikes/s d45 in PLL/Laminin), and lowest on Matrigel (D24 vs D45, **Fig. 6A**). In addition, the number of active electrodes continuously increased by time in culture, which followed a linear-

like trend for all coating conditions (Matrigel^{TM} R2 = 0.9319, LA R2 = 0.9003, PLL/LA R2 = 0.8780). When the MFF was evaluated only for the active electrodes, PLL/LA coating generated again showed the highest values on D45. (**Fig. 6A**).

Single Cell Patch Clamp Electrophysiology

To evaluate the baseline passive electrical properties of the cells, whole-cell patch-clamp recordings were performed on iNocs cultured on glass coverslips which only generated recordable cells when coated with Matrigel^{TM} and PLL/LA coating. Cell capacitance (C_m) and resting membrane potential (V_{rest}) were determined as measures of general excitability of the cell. There were no statistically significant differences in C_m between the Matrigel^{TM} and PLL/LA coating (Matrigel^{TM}: 11.82 ± 0.11 [n = 14] pF; PLL/LA: 13.56 pF ± 0.93 pF [n = 20]; n.s.) Similarly, the resting membrane potential was statistically indistinguishable between the different conditions (Matrigel^{TM}: -43.08 ± 3.33 mV [n = 17]; PLL/LA: -42.81 ± 2.4 mV [n = 17]; p = n.s.). In current-clamp recordings, spontaneous action potential (AP) activity was observed in only five cells: two cells cultured on Matrigel^{TM} coating (firing a total of two APs) and three cell cultured on PLL/LA coating (firing four APs). The spontaneous APs recorded from iNocs cultured on Matrigel^{TM} exhibited features indicating an immature neuronal phenotype (increased AP half-width (7.79 and 4.45 ms) and diminished peak amplitude (44.89 and 54.04 mV)) suggesting underdeveloped voltage-gated ion channel functionality, typical of premature neurons. APs recorded from two iNocs on PLL/LA showed more advanced AP characteristics and both total amplitude (81.63-87.33 mV) and half-width (1.73-1.95 ms) resembled those of human native nociceptors[32–34], and one cell generated two APs with parameters resembling an immature phenotype with a maximum amplitude of 52-53 mV. Interestingly one cell displayed a train of 13 APs in total, with a total amplitude between 52.19 and 78.22 mV, half-width between 1.62 and 2.27 ms and a mean firing frequency of 11.88 Hz. (**Fig. 6B**) Due to the rare abundance of spontaneous discharge activity no statistical tests were performed[33].

The kinetics of current-voltage recordings were also almost indistinguishable as the investigated parameters namely V_{rev} (Matrigel^{TM}: 92.31 ± 6.64 mV, PLL/LA: 98.63 ± 5.88 mV), $V_{0.5,max}$ (Matrigel^{TM}: -31.76 ± 1.18 mV, PLL/LA: -32.42 ± 1.25 mV), slope (Matrigel^{TM}: 2.39 ± 0.48 mV, PLL/LA: 2.00 ± 0.45 mV), maximum current density of the inward current (Matrigel^{TM}: -264.87 ± 24.68 pA/pF, PLL/LA: -221.10 ± 19.55 pA/pF) and maximum current density of the outward current (Matrigel^{TM}: 585.93 ± 83.13 pA/pF, PLL/LA: 41.317 ± 47.25

pA/pF) did not show any statistically significant differences (n = 11 for both groups, Mann-Whitney u-test, p = 0.0759; **Fig. 6C**).

Discussion and conclusion

In this study, surface coatings not only affected the morphology of iPSC derived nociceptors, but also strongly impacted on iNocs' transcriptomic profiles and cellular processes such as ion channel composition and, consequently, on pathways related to neuronal function and excitability. This was reflected by minor differences in electrophysiological properties and not surprising since native neurons and the cells surrounding them such as Schwann cells or satellite glia cells are firmly linked to ECM stabilizing their architecture; and neuronal interaction with the ECM initiates molecular signaling cascades impacting on neuronal development, morphology and function in health and disease[35–37].

LA is a major component of ECM and binds primarily to β1 containing integrin heterodimers on the cell surface such as α1β1, α3β1, α6β1 to activate MAPK/ERK and PI3K/Akt signaling pathways in outside-in signaling[38,39]. LA signaling cascades regulate cytoskeletal dynamics, neuronal survival, and gene transcription associated with neuronal maturation. and influences ion channel expression and excitability in sensory neurons, thereby linking ECM interactions to functional neuronal properties[40]. LA induces prominent neurite growth in cultured adult DRG neurons compared to other coating materials such as on thrombospondin, vitronectin, collagen type IV and fibronectin[41]. For iPSC derived neuronal models, a solubilized basement membrane preparation has been extracted from the Engelbreth-Holm-Swarm (EHS) mouse sarcoma, which is rich in ECM proteins such as LA, collagen IV, heparan sulfate proteoglycans, entactin/nidogen, and growth factors and routinely in use as Matrigel™ [42].Our morphological and sequencing analyses indicated that Matrigel coating was more prominently improving adhesion signaling and mesenchymal-associated transcriptional programs while suppressing neuronal differentiation-associated gene expression compared to other coatings. These transcriptional signatures suggested that the complex ECM composition of Matrigel™ may activate signaling pathways typically associated with tissue remodeling and cell migration not only in cortical iPSC derived neurons but also in iNocs[43].

Despite numerous studies on the physiological role of natural ECM components, synthetic polymers such as PLL are commonly used in cell cultures to screen negatively charged culture surfaces and provide better attachment in a nonreceptor mediated and unspecific manner through electrostatic interactions with negatively charged groups on both the culture surface and the cell membrane, thereby enhancing initial cell adhesion[44]. PLL coating renders the

plastic surface more hydrophilic and improves protein adsorption[45]. Beyond nonspecific attachment, the cationic surface increases adsorption and favorable orientation of ECM proteins such as LA and fibronectin, which in turn strengthen integrin-mediated signaling[38,39]. PLL/LA promotes cell cycle and proliferative transcriptional programs and maintains partial neuronal developmental signatures compared to Matrigel™. Laminin coating is associated with relatively reduced proliferation and ECM remodeling transcriptional signatures[38,39]. Regarding iNoc morphology, Matrigel™ and PLL/LA yielded comparable total cell numbers, while LA alone compared to Matrigel ™ yielded a significantly lower number of cells, indicating an important role of surface charge in iNoc adhesion. This suggested that surface charges provided by PLL may enhance the efficiency of ECM protein presentation and cell attachment, thereby improving survival of iNocs.

In vitro, iPSC derived neurons tend to passively form cell clusters even in the absence of glial cells or neuronal activity, which likely is driven by mechanical tension generated by extending neurites gradually pulling at cell bodies and producing spatially organized aggregates[46,47]. Numerous factors affect this clustering behavior such as cell seeding density, presence of glial cells, coating material and neuronal activity[39]. In turn, cell-cell contacts modulate neural cell adhesion molecules (NCAMs) and cadherins, which promote cytoskeletal coupling and stabilize neurite contacts[48,49]. We found formation of significantly larger clusters with LA, PLL/LA, collagen and carbon/gelatin coatings. Collagen and its derivative gelatin contain various cell recognition motifs stimulating cell-substrate interaction[50]. For example, collagen contains integrin-binding sequences such as the GFOGER motif, which can promote strong adhesion and potentially influence cell migration and aggregation behavior. The enhanced clustering observed with collagen-containing substrates may reflect increased integrin engagement and cytoskeletal tension within neuronal populations.

About two thirds of core matrisome genes (glycoproteins, collagens, and proteoglycans) and matrisome-associated genes (ECM-affiliated genes, ECM regulators, and secreted factors) are expressed in both murine and human DRG[51]. Of these, some of the core matrisome genes are linked to DE ion channels subtypes suggesting a critical role of ECM for neuronal excitability synaptic transmission and action potential generation[51–54]. Under physiological conditions, DRG neurons are not spontaneously active but rather show activity only when exposed to relevant stimuli. However, spontaneous activity in iPSC-derived nociceptors is well-documented[27,55]. Some of the tested coatings increased AP firing frequency, and this is in line with

previous studies reporting that ECM-integrin signaling influences neuronal excitability by regulating voltage-gated sodium and calcium channels[56]. In our patch-clamp recordings, coating materials influenced spontaneous AP firing and kinetics but did not alter passive membrane properties such as C_m and V_{rest}. Both examined parameters were far from typical physiological values [32–34], likely reflecting early-stage developmental deficits rather than a mature phentoype. The reduced AP amplitudes and prolonged AP half-widths on Matrigel™ strongly imply underdeveloped voltage-gated sodium or potassium channel kinetics[33,57,58]. Conversely, the transition toward higher AP peak amplitudes and narrower AP half-widths on PLL/LA coating suggested that this specific coating material provided a more supportive microenvironment for the maturation of active voltage-gated currents. To identify the individual contribution of specific voltage-gated ion channels, further studies need to clarify the exact contribution of individual ionic conductance and specific ion channel subtypes and assess whether alterations impact on different iPSC cell lines in a comparable manner. Increased spontaneous activity needs to be interpreted cautiously, since native DRG neurons are typically silent at baseline, spontaneous discharge is rare and increased action potential firing may reflect altered excitability rather than maturation per se. Additional comparison with different iPSC cell lines and multiple independent differentiations would be beneficial.

Together, these findings suggest that the coating material composition differentially modulated iNocs state possibly by regulating ECM signalling, proliferation, and lineage-associated transcriptional programs. Importantly, these effects extended beyond simple morphological differences and appeared to influence functional neuronal properties, the transcriptional identity and the molecular mechanisms underlying these changes with regards to ECM remains to be elucidated.

Funding

The authors sincerely thank the Medical University of Innsbruck for funding this study and supporting the research activities that contributed to this work. The research was supported in whole, or in part, by the Stiftung Aktion Österreich-Ungarn OMAA (grant number 114öu3 to MK and AS) and the Austrian Pain Society (Research grant 2025 to MK) and the Austrian Science Fund FWF (grant number I-5087 to MK).

K.P. was supported by TKP-NVA-20, FK_23_146912, the European Union's Horizon 2020 research and innovation programme (grant agreement No. 739593), and the Hungarian Research Network (HUN-REN) Supported Research Group Program 2024 (TKCS-2024/37). TKP-NVA-20 was funded by the Hungarian Ministry of Innovation and Technology through the National Research, Development and Innovation Fund under the TKP funding scheme. A.Sz. was supported by the National Research, Development and Innovation Fund (ANN_135291).

Data and code availability

The raw RNA-seq data generated in this study are available at the European Nucleotide Archive (ENA) under study accession number PRJEB128515. All custom code and software pipelines developed for data preprocessing, formal analysis, and visualization will be publicly available on GitHub.

Figure Captions:

Figure 1. Cell density evaluation of iNocs on different coatings. (A) Scanned coverslips of iNocs cultured on different coatings at D26. Scale bar represents 100 µm. (B) Percentage of the area covered by TUJ1+ staining on coverslips. Average fluorescence intensities were quantified using ImageJ software with a global threshold. Imaging and quantification was conducted in a blinded manner. All groups were compared to Matrigel. (One-way ANOVA with multiple comparisons). Scale bar represents 1 mm. (C) Normalized fluorescence intensity of neurons (TUJ1/DAPI) per coverslip. *p<0.05, **p<0.01, ***p<0.001.

Figure 2. Morphological analysis of iNocs on different coatings. (A) Quantification of total number of cells and percentage of neurons based on the total number of TUJ1+ cells compared to DAPI+ cells in D26 iNocs. Scale bar represents 100 µm. (B) Clustering behaviors of iNocs on different coverslips were evaluated compared to Matrigel by evaluation of percentage of single neurons compared to total TUJ1+ neurons and number of TUJ1+ cell clusters. (C) Mean number of TUJ1+ cells in clusters (D) Distribution of number of cells in each cluster for different coatings compared to Matrigel. (One-way ANOVA with multiple comparisons). p<0.05, **p<0.01, ***p<0.001

Figure 3. Transcriptomic Differences induced by LA, PLL_LA and Matrigel™. (A) PCA has been performed between samples from iNocs cultured on LA, Matrigel™ (MG) and PLL_LA. (B-D) Contrasted Pairwise Differential Expression analysis for different coating materials (B) Matrigel™ vs LA, (C) Matrigel™ vs PLL_LA, (D) PLL_LA vs LA. p<0.05, **p<0.01, ***p<0.001

Figure 4. Gene Ontology and Ion Channel Analysis. Different coating materials resulted in different gene profiles of iNocs. Gene Enrichment Ontology Analysis was performed for (A) up- and (B) downregulated Ontologies on Matrigel™ vs LA, (D) up- and (E) downregulated Ontologies in Matrigel™ vs PLL_LA and (G) up- and (H) downregulated Ontologies in PLL_LA vs LA. In addition, the number of up- and downregulated ion channels was analyzed for (C) Matrigel™ vs LA, (F) Matrigel™ vs PLL_LA and (I) PLL_LA vs LA. p<0.05, **p<0.01, ***p<0.001

Figure 5. iPSC-derived human nociceptors exhibit stable but asynchronous firing patterns that depend on the type of surface coating. The spike raster plots (A, C, E) demonstrate the firing activity of iNocs in three separate wells each containing 16 electrodes and recorded for 1000 s. Selected 200 s sections are indicated by the yellow rectangles and plotted on the

corresponding panels on the right. Spike density functions (firing frequency in Hz, light red, green and light blue) of the selected channels are plotted above the spike rasters. The spike trains produced by iNocs grown on Matrigel^{TM} (B), LA (D) and PLL/LA (F) surfaces are all independent for different recording channels. We observe slow oscillatory firing patterns in two of the demonstrated spike trains (top channel in B, 100 s period; bottom channel in F, 60 s period). However, the majority of the recorded channels display sporadic, random and low frequency firing.

Figure 6. Functional Differences induced by LA, PL_LA and Matrigel^{TM}**.** (A) iNocs on MEA electrodes coated with Matrigel^{TM}, laminin and PLL/laminin at d45. (B) Mean firing rate of iNocs on Matrigel^{TM}, LA and PLL/LA until d45 in culture per wells and per electrodes. (C) Percentage of active electrodes that showed at least an action potential per 10 min is increased by time for all coatings. (D) Peak inward (Ii) and outward (I_O) currents were measured and plotted to the corresponding membrane holding potential. Data are presented as mean ± SEM. Representative traces indicate a single action potential and a repetitive action potential recorded as spontaneous activity where cells were kept in current-clamp configuration with 0 pA current injection. $p<0.05$, $^{**}p<0.01$, $^{***}p<0.001$

References

1. Usoskin, D. *et al.* Unbiased classification of sensory neuron types by large-scale single-cell RNA sequencing. *Nat Neurosci* **18**, 145–153 (2015).

2. Li, C. L. *et al.* Somatosensory neuron types identified by high-coverage single-cell RNA-sequencing and functional heterogeneity. *Cell Res* **26**, 83–102 (2016).

3. Wang, K. *et al.* Single-cell transcriptomic analysis of somatosensory neurons uncovers temporal development of neuropathic pain. *Cell Res* **31**, 904–918 (2021).

4. Kupari, J. *et al.* Single cell transcriptomics of primate sensory neurons identifies cell types associated with chronic pain. *Nat Commun* **12**, 1510 (2021).

5. Nguyen, M. Q., von Buchholtz, L. J., Reker, A. N., Ryba, N. J. & Davidson, S. Single-nucleus transcriptomic analysis of human dorsal root ganglion neurons. *Elife* **10**, (2021).

6. Tavares-Ferreira, D. *et al.* Spatial transcriptomics of dorsal root ganglia identifies molecular signatures of human nociceptors. *Sci Transl Med* **14**, eabj8186 (2022).

7. Middleton, S. J. *et al.* Studying human nociceptors: from fundamentals to clinic. *Brain* **144**, 1312–1335 (2021).

8. Ray, P. *et al.* Comparative transcriptome profiling of the human and mouse dorsal root ganglia: an RNA-seq-based resource for pain and sensory neuroscience research. *Pain* **159**, 1325–1345 (2018).

9. Lopes, D. M., Denk, F. & McMahon, S. B. The Molecular Fingerprint of Dorsal Root and Trigeminal Ganglion Neurons. *Front Mol Neurosci* **10**, 304 (2017).

10. Schoepf, C. L. *et al.* Selected Ionotropic Receptors and Voltage-Gated Ion Channels: More Functional Competence for Human Induced Pluripotent Stem Cell (iPSC)-Derived Nociceptors. *Brain Sci* **10**, (2020).

11. Zeidler, M., Kummer, K. K. & Kress, M. Towards bridging the translational gap by improved modeling of human nociception in health and disease. *Pflugers Arch* **474**, 965–978 (2022).

12. Chambers, S. M. *et al.* Combined small-molecule inhibition accelerates developmental timing and converts human pluripotent stem cells into nociceptors. *Nat Biotechnol* **30**, 715–720 (2012).

13. Zeidler, M. *et al.* NOCICEPTRA: Gene and microRNA Signatures and Their Trajectories Characterizing Human iPSC-Derived Nociceptor Maturation. *Adv Sci (Weinh)* **8**, e2102354 (2021).

14. Zeidler, M., Tavares-Ferreira, D., Brougher, J., Price, T. J. & Kress, M. NOCICEPTRA2.0 - A comprehensive ncRNA atlas of human native and iPSC-derived sensory neurons. *iScience* **26**, 108525 (2023).

15. Reichelt, A. C., Hare, D. J., Bussey, T. J. & Saksida, L. M. Perineuronal Nets: Plasticity, Protection, and Therapeutic Potential. *Trends Neurosci* **42**, 458–470 (2019).

16. Fudge, N. J. & Mearow, K. M. Extracellular matrix-associated gene expression in adult sensory neuron populations cultured on a laminin substrate. *BMC Neurosci* **14**, 15 (2013).

17. Chong, M. K., Cebul, E. R., Mizeracka, K. & Heiman, M. G. Loss of the Extracellular Matrix Protein DIG-1 Causes Glial Fragmentation, Dendrite Breakage, and Dendrite Extension Defects. *J Dev Biol* **9**, (2021).

18. Park, Y. K. & Goda, Y. Integrins in synapse regulation. *Nat Rev Neurosci* **17**, 745–756 (2016).

19. Silver, D. J. & Silver, J. Contributions of chondroitin sulfate proteoglycans to neurodevelopment, injury, and cancer. *Curr Opin Neurobiol* **27**, 171–178 (2014).

20. Álvarez, Z. *et al.* Artificial extracellular matrix scaffolds of mobile molecules enhance maturation of human stem cell-derived neurons. *Cell Stem Cell* **30**, 219-238.e14 (2023).

21. Shin, G. J. *et al.* Integrins protect sensory neurons in models of paclitaxel-induced peripheral sensory neuropathy. *Proc Natl Acad Sci U S A* **118**, (2021).

22. Alessandri-Haber, N., Dina, O. A., Joseph, E. K., Reichling, D. B. & Levine, J. D. Interaction of transient receptor potential vanilloid 4, integrin, and SRC tyrosine kinase in mechanical hyperalgesia. *J Neurosci* **28**, 1046–1057 (2008).

23. Liu, D. *et al.* Coating Materials for Neural Stem/Progenitor Cell Culture and Differentiation. *Stem Cells Dev* **29**, 463–474 (2020).

24. Sağraç, D. *et al.* Surface coating materials regulates the attachment and differentiation of mouse embryonic stem cell derived embryoid bodies into mesoderm at culture conditions. *Cytotechnology* **74**, 293–307 (2022).

25. Tay, S. H. *et al.* iPSC-derived human sensory neurons reveal a subset of TRPV1 antagonists as anti-pruritic compounds. *Sci Rep* **14**, 31182 (2024).

26. Guimarães, M. Z. P. *et al.* Generation of iPSC-Derived Human Peripheral Sensory Neurons Releasing Substance P Elicited by TRPV1 Agonists. *Front Mol Neurosci* **11**, 277 (2018).

27. Hiranuma, M., Okuda, Y., Fujii, Y., Richard, J. P. & Watanabe, T. Characterization of human iPSC-derived sensory neurons and their functional assessment using multi electrode array. *Sci Rep* **14**, 6011 (2024).

28. Fofie, C. K. *et al.* Profiling human iPSC-derived sensory neurons for analgesic drug screening using a multi-electrode array. *Cell Rep Methods* **5**, 101051 (2025).

29. Love, M. I., Huber, W. & Anders, S. Moderated estimation of fold change and dispersion for RNA-seq data with DESeq2. *Genome Biol* **15**, 550 (2014).

30. Ben Mahmoud, M. *et al.* Multifactorial approach is needed to unravel the maturation phases of human neurons derived from induced pluripotent stem cells. *Sci. Rep.* **15**, 2627 (2025).

31. Kalia, A. K. *et al.* How to differentiate induced pluripotent stem cells into sensory neurons for disease modelling: a functional assessment. *Stem Cell Res. Ther.* **15**, 99 (2024).

32. Davidson, S. *et al.* Human sensory neurons: Membrane properties and sensitization by inflammatory mediators. *Pain* **155**, 1861–1870 (2014).

33. North, R. Y. *et al.* Electrophysiological Alterations Driving Pain-Associated Spontaneous Activity in Human Sensory Neuron Somata Parallel Alterations Described in Spontaneously Active Rodent Nociceptors. *J Pain* **23**, 1343–1357 (2022).

34. North, R. Y. *et al.* Electrophysiological and transcriptomic correlates of neuropathic pain in human dorsal root ganglion neurons. *Brain* **142**, 1215–1226 (2019).

35. Long, K. R. & Huttner, W. B. The Role of the Extracellular Matrix in Neural Progenitor Cell Proliferation and Cortical Folding During Human Neocortex Development. *Front Cell Neurosci* **15**, 804649 (2021).

36. Kwok, J. C. F. & Dityatev, A. Extracellular matrix remodelling in neurological diseases. *Nat Rev Neurol* **22**, 366–384 (2026).

37. Ge, C. & Tajerian, M. The extracellular matrix as a dynamic regulator of brain function and plasticity. *Neurobiol Dis* **223**, 107374 (2026).

38. Gary, D. S. & Mattson, M. P. Integrin signaling via the PI3-kinase-Akt pathway increases neuronal resistance to glutamate-induced apoptosis. *J Neurochem* **76**, 1485–1496 (2001).

39. de Campos, C. C. *et al.* The relationship between symptoms and electrophysiological detected compression of the median nerve at the wrist. *Acta Neurol Scand* **110**, 398–402 (2004).

40. Myers, J. P., Santiago-Medina, M. & Gomez, T. M. Regulation of axonal outgrowth and pathfinding by integrin-ECM interactions. *Dev. Neurobiol.* **71**, 901–23 (2011).

41. Plantman, S. *et al.* Integrin-laminin interactions controlling neurite outgrowth from adult DRG neurons in vitro. *Mol Cell Neurosci* **39**, 50–62 (2008).

42. Kleinman, H. K. & Martin, G. R. Matrigel: basement membrane matrix with biological activity. *Semin Cancer Biol* **15**, 378–386 (2005).

43. Li, S., Liu, Y., Luo, X. & Hong, W. Systematic Evaluation of Extracellular Coating Matrix on the Differentiation of Human-Induced Pluripotent Stem Cells to Cortical Neurons. *Int. J. Mol. Sci.* **26**, (2024).

44. Wu, C. *et al.* Cellular and Molecular Insights into the Divergence of Neural Stem Cells on Matrigel and Poly-l-lysine Interfaces. *ACS Appl Mater Interfaces* **16**, 31922–31935 (2024).

45. Wang, Y. H., Chang, S. H., Mau-Hsu, D., Wang, J. H. & Young, T. H. Poly(N-(4-aminobutyl)-acrylamide) as mimetic polylysine for improving survival and differentiation of cerebellar granule neurons. *J Biomed Mater Res B Appl Biomater* **106**, 1194–1201 (2018).

46. Segev, R., Benveniste, M., Shapira, Y. & Ben-Jacob, E. Formation of electrically active clusterized neural networks. *Phys Rev Lett* **90**, 168101 (2003).

47. Teller, S. *et al.* Emergence of assortative mixing between clusters of cultured neurons. *PLoS Comput Biol* **10**, e1003796 (2014).

48. Esch, T., Lemmon, V. & Banker, G. Differential effects of NgCAM and N-cadherin on the development of axons and dendrites by cultured hippocampal neurons. *J Neurocytol* **29**, 215–223 (2000).

49. Maness, P. F. & Schachner, M. Neural recognition molecules of the immunoglobulin superfamily: signaling transducers of axon guidance and neuronal migration. *Nat Neurosci* **10**, 19–26 (2007).

50. Heino, J. The collagen family members as cell adhesion proteins. *Bioessays* **29**, 1001–10 (2007).

51. Vroman, R. *et al.* Analysis of matrisome expression patterns in murine and human dorsal root ganglia. *Front Mol Neurosci* **16**, 1232447 (2023).

52. Girard, C. *et al.* p11, an annexin II subunit, an auxiliary protein associated with the background K+ channel, TASK-1. *Embo j* **21**, 4439–4448 (2002).

53. Chan, C. S. *et al.* Beta 1-integrins are required for hippocampal AMPA receptor-dependent synaptic transmission, synaptic plasticity, and working memory. *J Neurosci* **26**, 223–232 (2006).

54. Michaluk, P. *et al.* Matrix metalloproteinase-9 controls NMDA receptor surface diffusion through integrin beta1 signaling. *J Neurosci* **29**, 6007–6012 (2009).

55. Odawara, A. *et al.* In Vitro Pain Assay Using Human iPSC-Derived Sensory Neurons and Microelectrode Array. *Toxicol Sci* **188**, 131–141 (2022).

56. Dityatev, A. & Schachner, M. Extracellular matrix molecules and synaptic plasticity. *Nat Rev Neurosci* **4**, 456–468 (2003).

57. Nascimento, A. I. *et al.* Sensory neurons have an axon initial segment that initiates spontaneous activity in neuropathic pain. *Brain* **145**, 1632–1640 (2022).

58. Choi, D. *et al.* Spontaneous activity in peripheral sensory nerves: a systematic review. *Pain* **165**, 983–996 (2024).

Additional information:

Author contribution statement:

Each author has made substantial contributions and has approved the submitted version. They have agreed both to be personally accountable for their own contributions and ensure that questions related to the accuracy or integrity of any part of the work, even ones in which they were not personally involved, are appropriately investigated, resolved, and the resolution documented in the literature. Conception and design of the work: BU, DZ, FT, AS, MK; Acquisition, analysis, and interpretation of data: BU, DZ, FT, GK, AS; Creation of new software used in the work: DZ; Manuscript draft and revision: BU, DZ, FT, KP, AS, MK.

Competing interests statement:

The author(s) declare no competing interests.

Figure 1

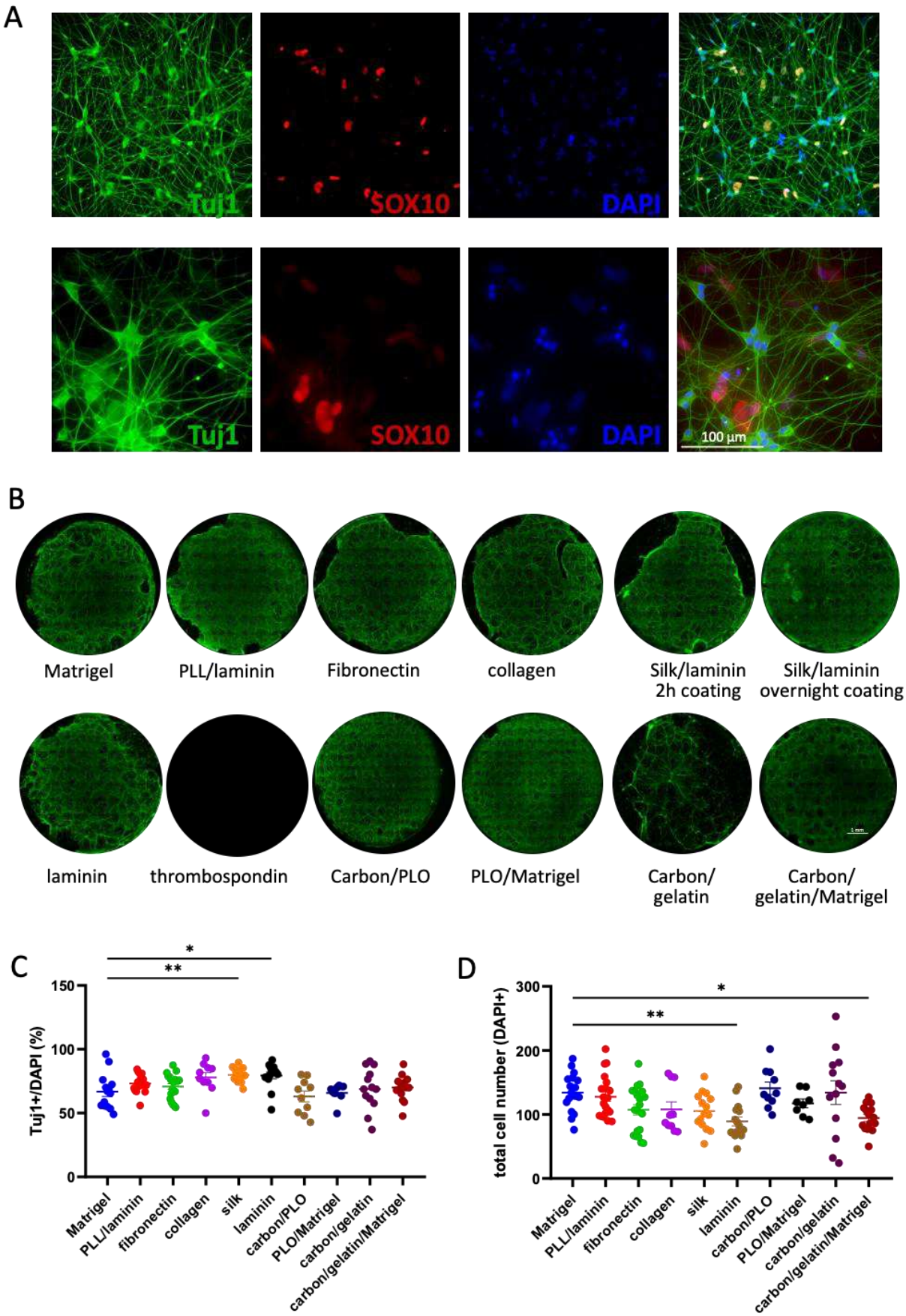

A
Tuj1
SOX10
DAPI
Tuj1
SOX10
DAPI
100 µm
B
Matrigel
PLL/laminin
Fibronectin
collagen
Silk/laminin 2h coating
Silk/laminin overnight coating
laminin
thrombospondin
Carbon/PLO
PLO/Matrigel
Carbon/ gelatin
Carbon/ gelatin/Matrigel
C
Tuj1+/DAPI (%)
150
100
50
0
*
**
Matrigel
PLL/laminin
fibronectin
collagen
silk
laminin
carbon/PLO
PLO/Matrigel
carbon/gelatin
carbon/gelatin/Matrigel
D
total cell number (DAPI+)
300
200
100
0
*
**
Matrigel
PLL/laminin
fibronectin
collagen
silk
laminin
carbon/PLO
PLO/Matrigel
carbon/gelatin
carbon/gelatin/Matrigel

Figure 2

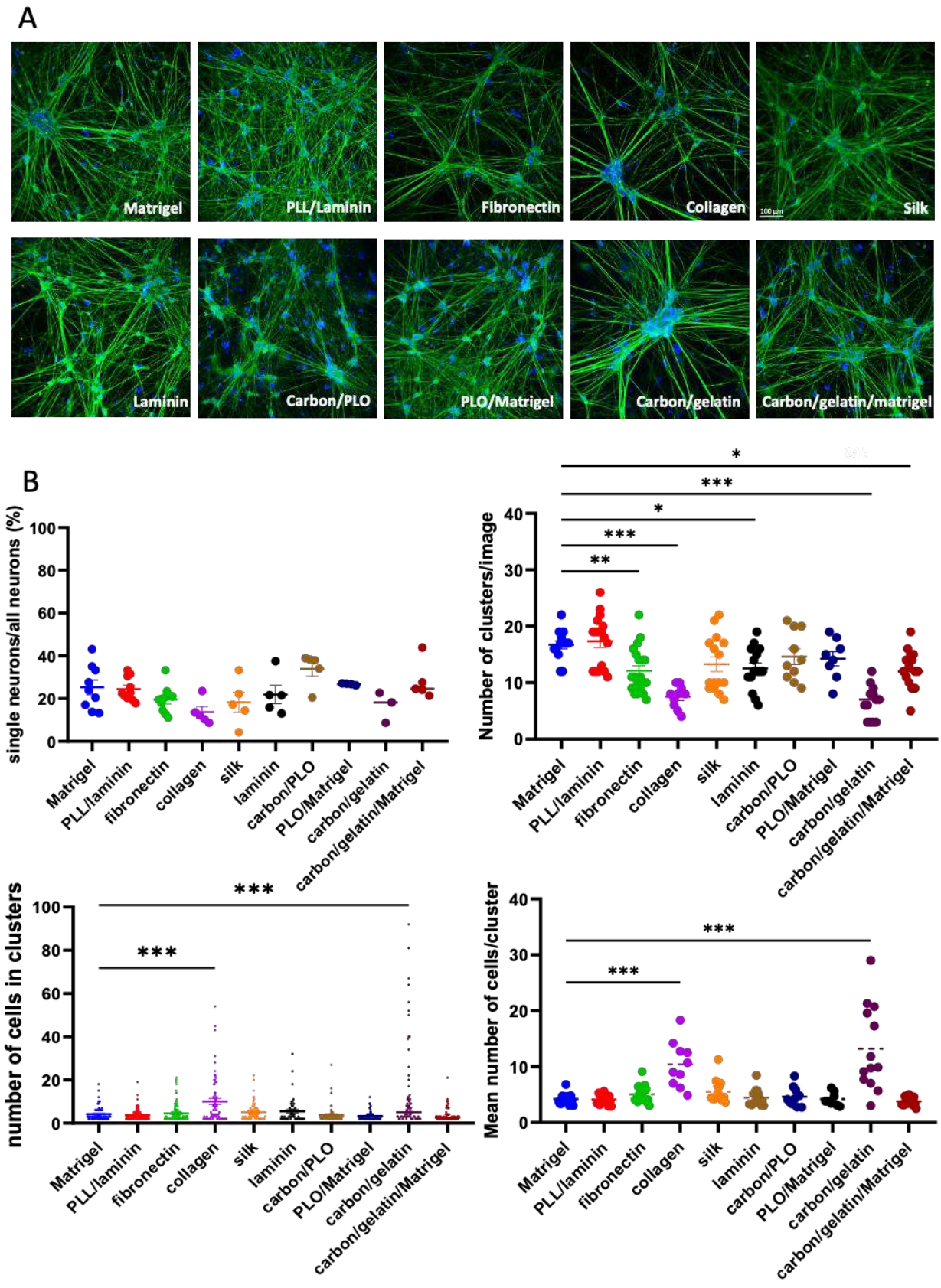

A
Matrigel
PLL/Laminin
Fibronectin
Collagen
Silk
Laminin
Carbon/PLO
PLO/Matrigel
Carbon/gelatin
Carbon/gelatin/matrigel
B
single neurons/all neurons (%)
Number of clusters/image
number of cells in clusters
Mean number of cells/cluster
Matrigel
PLL/laminin
fibronectin
collagen
silk
laminin
carbon/PLO
PLO/Matrigel
carbon/gelatin
carbon/gelatin/Matrigel

Figure 3

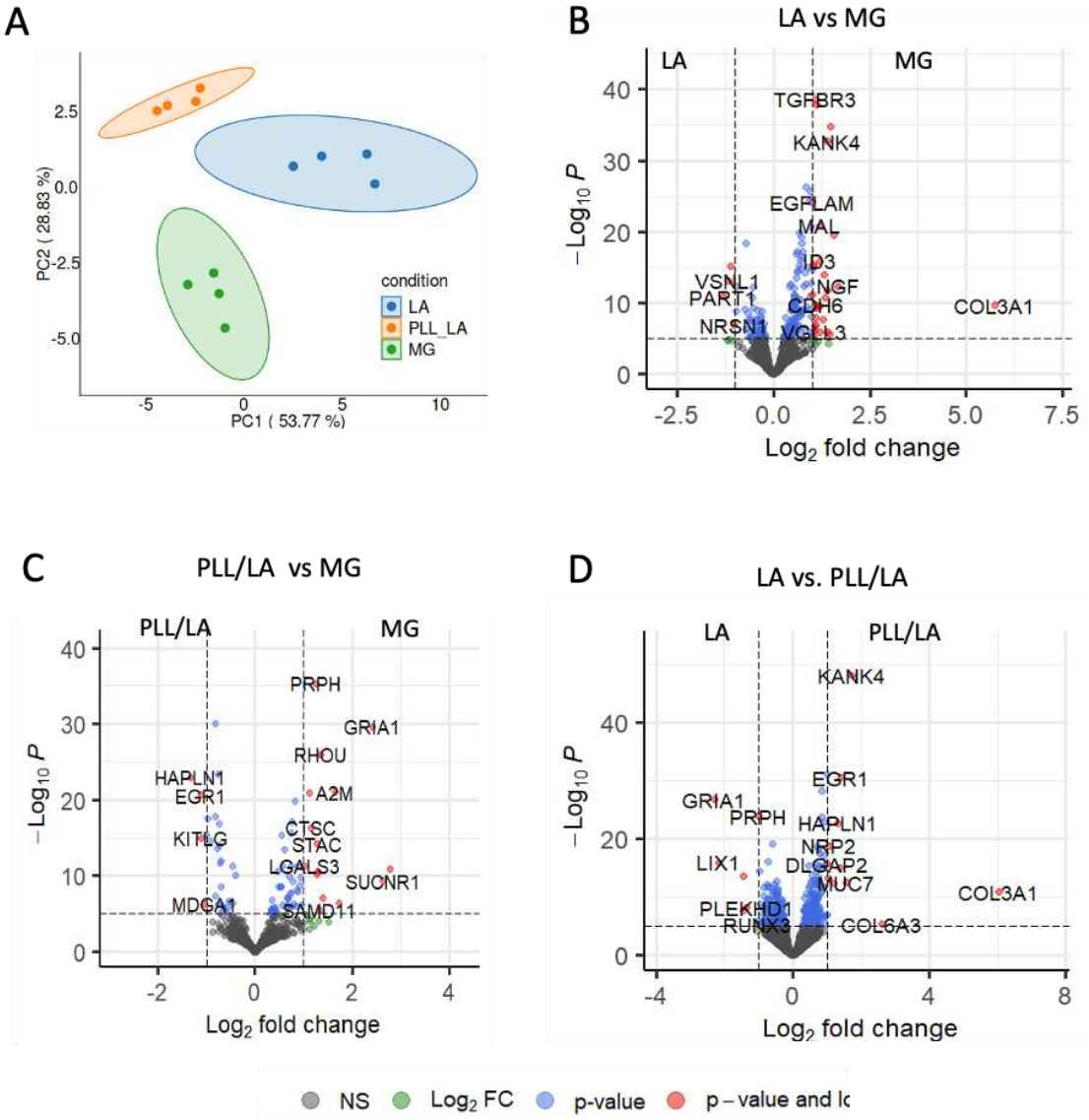

A
PC2 (28.83 %)
PC1 (53.77 %)
condition
LA
PLL_LA
MG
B
LA vs MG
LA
MG
TGFBR3
KANK4
EGFLAM
MAL
ID3
NGF
VSNL1
PART1
CDH6
NRSN1
VGLL3
COL3A1
$-\mathrm{Log}_{10}P$
Log_2 fold change
C
PLL/LA vs MG
PLL/LA
MG
PRPH
GRIA1
RHOU
HAPLN1
EGR1
A2M
CTSC
KITLG
STAC
LGALS3
SUCNR1
MDGA1
SAMD11
$-\mathrm{Log}_{10}P$
Log_2 fold change
D
LA vs. PLL/LA
LA
PLL/LA
KANK4
EGR1
GRIA1
PRPH
HAPLN1
NRP2
LIX1
DLGAP2
MUC7
COL3A1
PLEKHD1
RUNX3
COL6A3
$-\mathrm{Log}_{10}P$
Log_2 fold change
NS
Log_2 FC
p-value
p – value and lc

Figure 4

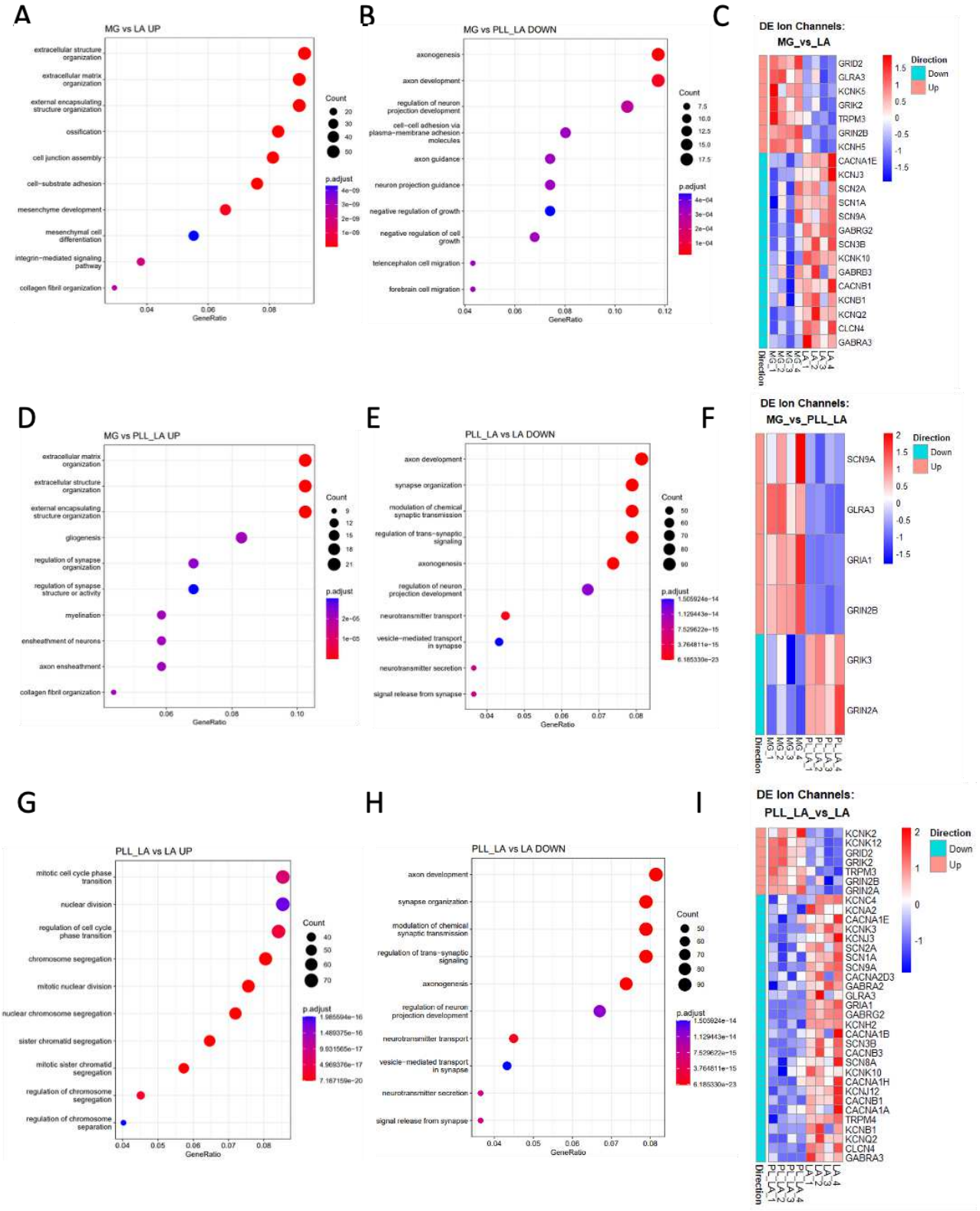

A
MG vs LA UP
extracellular structure organization
extracellular matrix organization
external encapsulating structure organization
ossification
cell junction assembly
cell−substrate adhesion
mesenchyme development
mesenchymal cell differentiation
integrin−mediated signaling pathway
collagen fibril organization
GeneRatio
Count
p.adjust
B
MG vs PLL_LA DOWN
axonogenesis
axon development
regulation of neuron projection development
cell−cell adhesion via plasma−membrane adhesion molecules
axon guidance
neuron projection guidance
negative regulation of growth
negative regulation of cell growth
telencephalon cell migration
forebrain cell migration
GeneRatio
Count
p.adjust
C
DE Ion Channels:
MG_vs_LA
GRID2
GLRA3
KCNK5
GRIK2
TRPM3
GRIN2B
KCNH5
CACNA1E
KCNJ3
SCN2A
SCN1A
SCN9A
GABRG2
SCN3B
KCNK10
GABRB3
CACNB1
KCNB1
KCNQ2
CLCN4
GABRA3
Direction
Down
Up
D
MG vs PLL_LA UP
extracellular matrix organization
extracellular structure organization
external encapsulating structure organization
gliogenesis
regulation of synapse organization
regulation of synapse structure or activity
myelination
ensheathment of neurons
axon ensheathment
collagen fibril organization
GeneRatio
Count
p.adjust
E
PLL_LA vs LA DOWN
axon development
synapse organization
modulation of chemical synaptic transmission
regulation of trans−synaptic signaling
axonogenesis
regulation of neuron projection development
neurotransmitter transport
vesicle−mediated transport in synapse
neurotransmitter secretion
signal release from synapse
GeneRatio
Count
p.adjust
F
DE Ion Channels:
MG_vs_PLL_LA
SCN9A
GLRA3
GRIA1
GRIN2B
GRIK3
GRIN2A
Direction
Down
Up
G
PLL_LA vs LA UP
mitotic cell cycle phase transition
nuclear division
regulation of cell cycle phase transition
chromosome segregation
mitotic nuclear division
nuclear chromosome segregation
sister chromatid segregation
mitotic sister chromatid segregation
regulation of chromosome segregation
regulation of chromosome separation
GeneRatio
Count
p.adjust
H
PLL_LA vs LA DOWN
axon development
synapse organization
modulation of chemical synaptic transmission
regulation of trans−synaptic signaling
axonogenesis
regulation of neuron projection development
neurotransmitter transport
vesicle−mediated transport in synapse
neurotransmitter secretion
signal release from synapse
GeneRatio
Count
p.adjust
I
DE Ion Channels:
PLL_LA_vs_LA
KCNK2
KCNK12
GRID2
GRIK2
TRPM3
GRIN2B
GRIN2A
KCNC4
KCNA2
CACNA1E
KCNK3
KCNJ3
SCN2A
SCN1A
SCN9A
CACNA2D3
GABRA2
GLRA3
GRIA1
GABRG2
KCNH2
CACNA1B
SCN3B
CACNB3
SCN8A
KCNK10
CACNA1H
KCNJ12
CACNB1
CACNA1A
TRPM4
KCNB1
KCNQ2
CLCN4
GABRA3
Direction
Down
Up

Figure 5

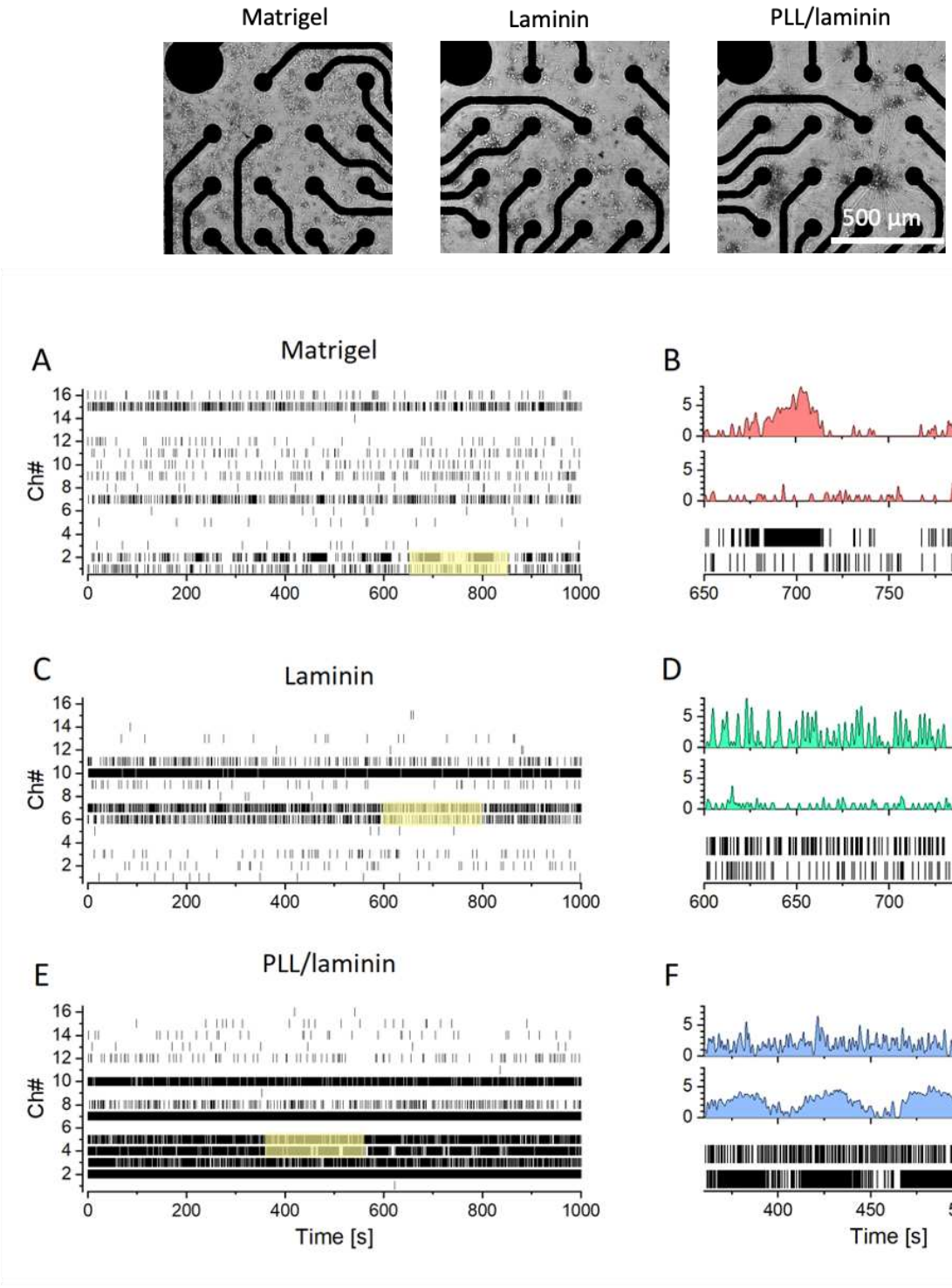
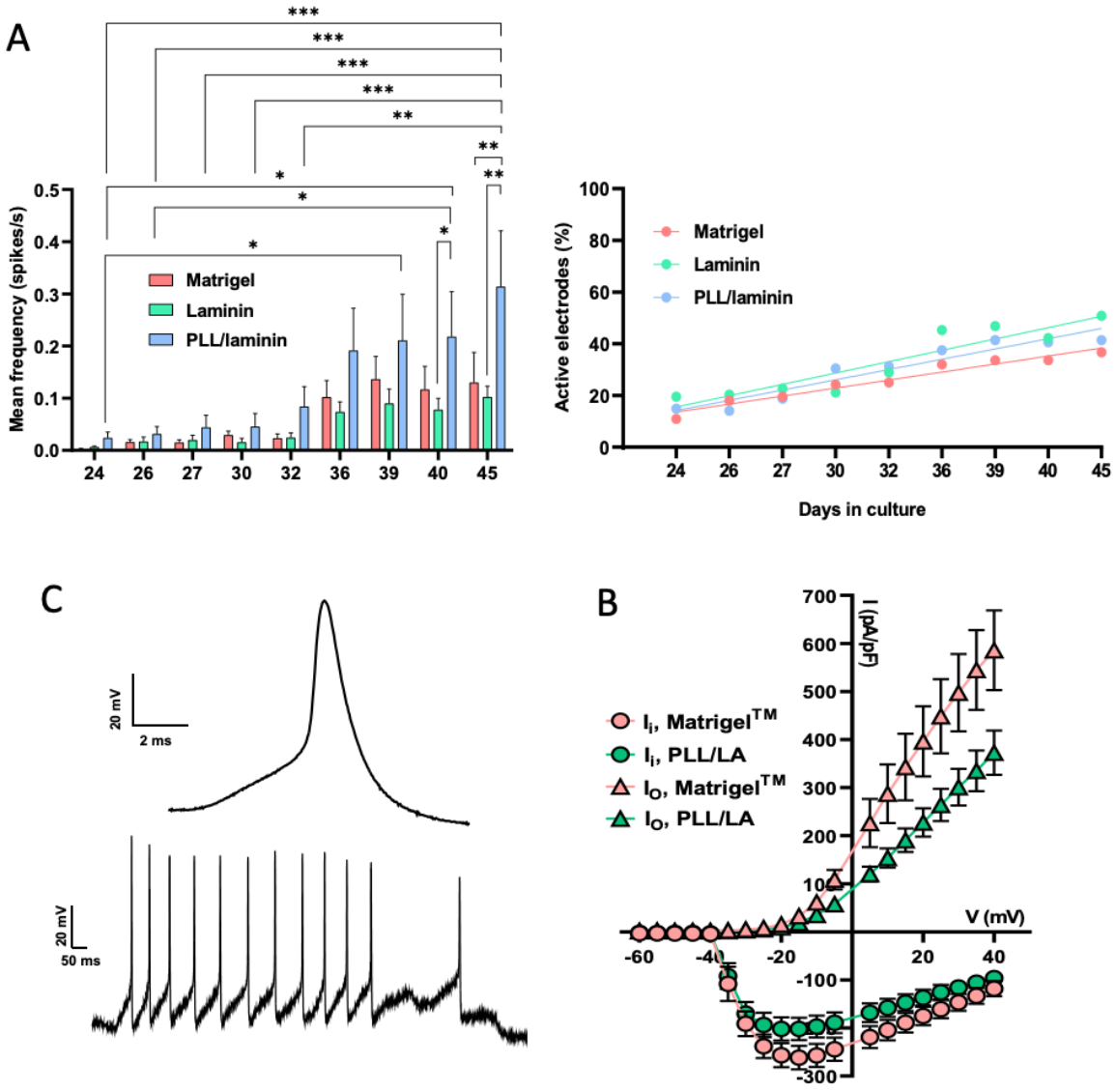

Matrigel
Laminin
PLL/laminin
500 µm
A
Matrigel
Ch#
B
C
Laminin
D
E
PLL/laminin
F
Time [s]
Time [s]

Figure 6


A
Mean frequency (spikes/s)
Matrigel
Laminin
PLL/laminin
24 26 27 30 32 36 39 40 45
Active electrodes (%)
Days in culture
C
20 mV
2 ms
20 mV
50 ms
B
I (pA/pF)
V (mV)
I_i, Matrigel™
I_i, PLL/LA
I_O, Matrigel™
I_O, PLL/LA